arXiv:1601.07225v1 [stat.AP] 26 Jan 2016

Wavelet Analysis in a Canine Model of Gastric Electrical Uncoupling

R. J. Cintra* I. V. Tchervensky† V. S. Dimitrov‡ M. P. Mintchev§

Abstract

Abnormal gastric motility function could be related to gastric electrical uncoupling, the lack of electrical, and respectively mechanical, synchronization in different regions of the stomach. Therefore, non-invasive detection of the onset of gastric electrical uncoupling can be important for diagnosing associated gastric motility disorders. The aim of this study is to provide a wavelet-based analysis of electrogastrograms (EGG, the cutaneous recordings of gastric electric activity), to detect gastric electric uncoupling. Eight-channel EGG recordings were acquired from sixteen dogs in basal state and after each of two circular gastric myotomies. These myotomies simulated mild and severe gastric electrical uncoupling, while keeping the separated gastric sections electrophysiologically active by preserving their blood supply. After visual inspection, manually selected 10-minute EGG segments were submitted to wavelet analysis. Quantitative methodology to choose an optimal wavelet was derived. This "matching" wavelet was determined using the Pollen parameterization for 6-tap wavelet filters and error minimization criteria. After a wavelet-based compression, the distortion of the approximated EGG signals was computed. Statistical analysis on the distortion values allowed to significantly ($p < 0.05$) distinguish basal state from mild and severe gastric electrical uncoupling groups in particular EGG channels.

Keywords

Electrogastrography, wavelet analysis, signal classification

1 Introduction

Gastric electrical activity (GEA) controls the motility of the stomach [1, 2]. Gastric motility disorders, including functional gastroparesis and dyspepsia, have been related to alterations in GEA dynamics [3]. Abnormal GEA could be regarded as a result of two different phenomena: (i) global gastric electrical dysrhythmias encompassing simultaneously the entire organ; and (ii) local gastric electrical dysrhythmias, often manifesting themselves as gastric electrical uncoupling.

Many studies emphasized the impact of alterations in the GEA rhythm as the main reason for gastric motility abnormalities [4–6]. However, global gastric dysrhythmias are by themselves uncommon and have

*R. J. Cintra was with Graduate Program in Electrical Engineering, Universidade Federal de Pernambuco, Brazil. Currently, he is with the *Departamento de Estatística* at the same university. Email: rjdsc@de.ufpe.br

†I. V. Tchevensky was with the Department of Electrical and Computer Engineering, University of Calgary, Calgary, Alberta, Canada T2N 1N4.

‡V. S. Dimitrov is with the Department of Electrical and Computer Engineering, University of Calgary, Calgary, Alberta, Canada T2N 1N4, and with the Computer Modelling Group, Calgary.

§M. P. Mintchev is with the Department of Electrical and Computer Engineering, University of Calgary, Calgary, Alberta, Canada T2N 1N4 and the Department of Surgery, University of Alberta, Edmonton, Alberta, Canada T6G 2B7. Email: mintchev@ucalgary.ca

been objectively registered only incidentally [7,8]. Often, local dysrhythmias and gastric electrical uncoupling are simultaneously present and could be considered very similar, if not the same phenomena.

Gastric electrical uncoupling occurs when different parts of the stomach lose synchronization creating independent oscillating regions which are dysrhythmic with respect to the global GEA frequency [9]. In pure uncoupling these independent regions are characterized each with steady but different GEA rhythm. However, often this is not the case, and dysrhythmias are also present. Regardless whether the stomach is uncoupled or both uncoupled and locally dysrhythmic, the lack of oscillatory coordination leads to abnormal gastric motor function [10]. Therefore, the identification of gastric electrical uncoupling can be important in diagnosing gastric motility abnormalities [2].

In this context, cutaneous recordings of GEA, known as electrogastrography (EGG), can play a major role in the diagnosis of gastric motility disorders [11], since EGG was successfully related to gastric electrical uncoupling [12]. Because of its low-cost and non-invasiveness, the EGG technique has a great appeal as a clinical tool. Numerous studies had been conducted in order to classify EGG recordings of surgically produced gastric electrical uncoupling in large experimental animals. Such studies included examination of the level of randomness [13], the level of chaos [14], biomagnetic field patterns [9, 15, 16], and dominant frequency dynamics [12].

Separately, refined signal processing techniques, such as wavelets, have been employed to analyze electrogastrograms [17–21]. This approach has been used to (i) propose new wavelets that can offer a better time-frequency localization of EGG signals [17, 18]; (ii) perform noise detection in EGG recordings [19]; (iii) reduce stimulus artefacts [20]; and (iv) characterize global gastric electrical dysrhythmias [21].

In the present study, a new application of wavelets for EGG analysis in detecting gastric electrical uncoupling and local dysrhythmias is proposed. It is hypothesized that normal and uncoupled EGG recordings have different typical energy distribution throughout their wavelet transform coefficients. Thus, the quality assessment parameters of compressed normal and uncoupled electrogastrograms would be different, since distinct amounts of energy would be used in the signal reconstruction.

The aim of this study is to present a method to quantitatively detect mild and severe gastric electrical uncoupling using wavelet compression in a canine model.

2 Methods

2.1 Experimental Setup

After a laparotomy and the instalment of six pairs of internal subserosal stainless steel wire electrodes into the antral gastric wall of sixteen acute dogs (seven female and nine male), two complete circumferential cuts were made fully dividing the organ into separate sections, but preserving the blood supply in each. After each cut, the stomach was not anastomosed. The sites of the cuts were selected to be distal to the gastro-esophageal junction (first cut) and proximal to gastro-esophageal junction (second cut). Consequently, by the end of the experiment, these circular myotomies divided the stomach in three parts of approximately equal dimensions. Similar type of experimental work was described before [12–14].

After each incision, the abdominal wall was closed and five standard disposable neonatal electrocardiography Ag-AgCl electrodes (Conmed, Andover Medical, Haverhill, MA, USA) were collinearly placed on the abdominal wall along the projection of the gastric axis. Additionally a reference electrode was positioned in the area of

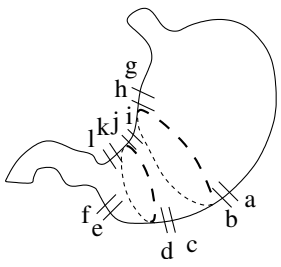

(a)

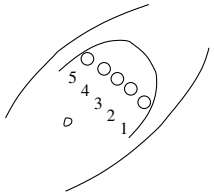

(b)

Channel	Electrode Combination
1	a–b
2	c–d
3	e–f
4	g–h
5	i–j
6	k–l

(c)

Channel	Electrode Combination
7	1–2
8	2–3
9	3–4
10	4–5
11	1–3
12	1–4
13	2–5
14	1–5

(d)

Figure 1: Internal (a) and cutaneous (b) electrode positioning. Various electrode combinations were used for the GEA (c) and the EGG (d) recordings.

the hip. Previous studies demonstrated that this electrode configuration can be regarded as optimal [22]. The five active electrodes were grouped to provide eight bipolar EGG channels. Furthermore, six stainless-steel wire electrodes implanted subserosally provided six bipolar channels of internal GEA. However, in the present study only the eight EGG recordings were processed, while the internal GEA channels were used as a visual reference only to verify that normal electrical activity was present. The electrode combination set and a diagram of the physical location of the electrodes are depicted on Figure 1.

Thirty-minute EGG recordings were performed in the three different states: (i) basal state; (ii) mild gastric electrical uncoupling (after the first cut); and (iii) severe gastric electrical uncoupling (after the second cut).

The captured EGG signals were conditioned by a 0.02–0.2 Hz low-pass first order Butterworth active filter. After amplification, 12-bit analog-to-digital conversion was performed using a sampling frequency of 10 Hz and Labmaster 20009 16-channel analog-to-digital converter (Scientific Solutions, Vancouver, BC, Canada). Thus, each half-hour recording generated 18,000 samples per channel per state (basal, mild uncoupling after the first cut, and severe uncoupling after the second cut) per dog.

All experiments were approved by the Animal Welfare Committee and the Ethics Committee at the Faculty of Medicine, University of Alberta (Edmonton, Alberta, Canada).

Since the recordings were of significant duration, the raw EGG data recordings were intermittently contaminated with a multitude of artefacts, including: (i) motion artefacts; (ii) spontaneous variations in electrode potentials; (iii) respiration; (iv) signal saturation during recording; (v) electrocardiac activity; and (vi) loss of signal during recording. Usually these artefacts appeared simultaneously in all recording channels. Figure 2 depicts examples of various categories of corrupted signals. Some of these noisy patterns were visually evident (e.g., iv and vi) and could be easily identified and discarded [23]. This practice has been recommended before in order to obtain a more reliable signal for subsequent analysis [6].

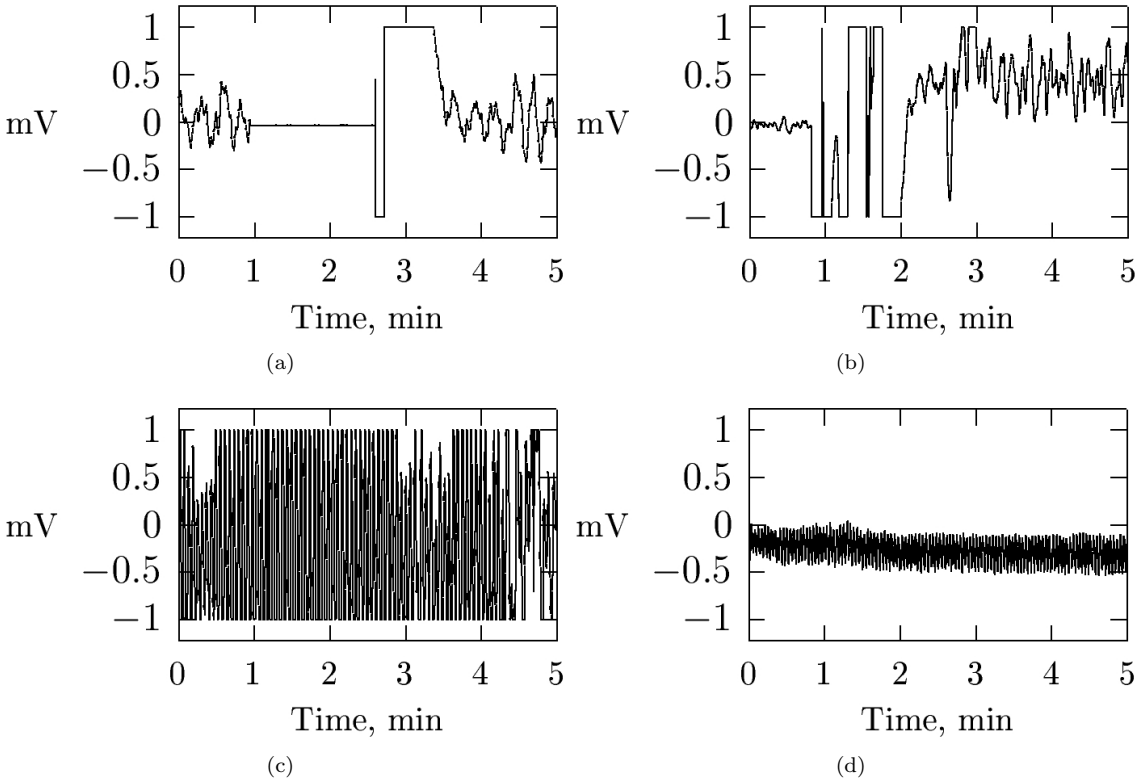

Figure 2: Examples of common artefacts found in raw EGG recordings: loss of signal (a), offset change and saturation (b), noise and saturation (c), and lack of signal due to technological problems (d).

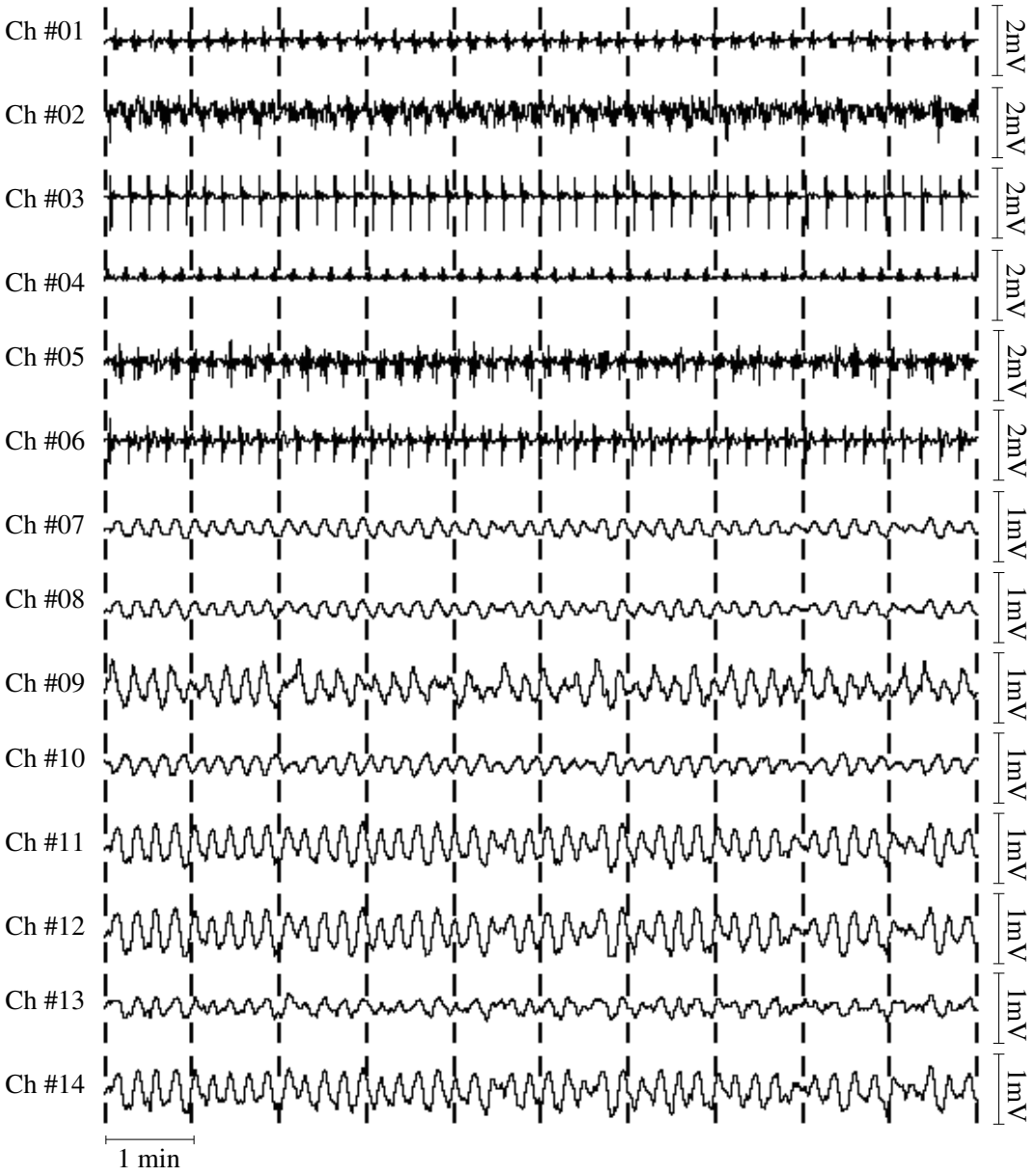

Figure 3: Typical multichannel electrogastrographic tracings in the basal state. Channels 1–6 are internal GEA, channels 7–14 are EGG.

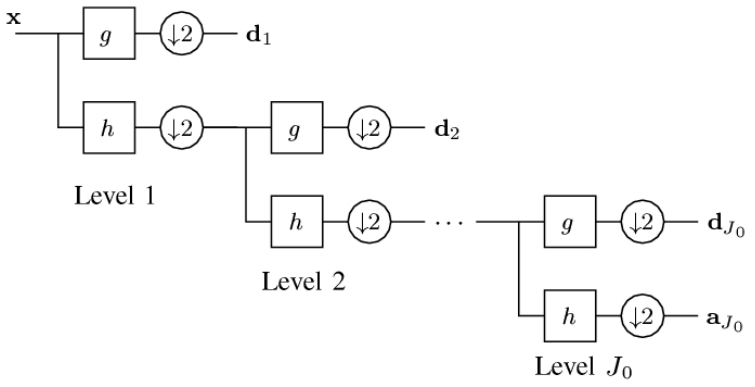

Figure 4: Wavelet analysis filter bank. The signal is iteratively decomposed through a filter bank to obtain its discrete wavelet transform.

Therefore, for each dog, a 10-minute time interval of channel-synchronized data was manually selected. These data were considered to be free from identifiable noise patterns. Figure 3 shows a typical 10-minute multichannel basal EGG recording.

2.2 Signal Analysis

2.2.1 Wavelet Compression

Wavelet theory suggests that it is possible to choose a wavelet function $\psi(\cdot)$ that generates an orthogonal basis in which a given signal is to be decomposed [24]. A continuous signal $x(t)$ has its wavelet transform coefficients $c_{j,k}$ computed by

$$c_{j,k} = \int_{-\infty}^{\infty} x(t)\psi_{j,k}(t)\mathrm{d}t, \tag{1}$$

where the basis $\psi_{j,k}(\cdot) = 2^{-j/2}\psi(2^{-j}\cdot - k)$ is controlled by a scale (dilation) integer index j and a translation integer index k.

Under some assumptions [24], these coefficients uniquely represent $x(t)$, which can be reconstructed by the following wavelet series

$$x(t) = \sum_{j=-\infty}^{\infty}\sum_{k=-\infty}^{\infty} c_{j,k}\psi_{j,k}(t). \tag{2}$$

Equation 2 represents the synthesis equation or inverse wavelet transform [25].

This transform has to be modified for processing digitized signals. Moreover, in a discrete-time formalism the direct definition of the wavelet transform is computationally intensive. Wavelet transforms are performed via the Fast Wavelet Transform using Mallat's pyramid algorithm for decomposition (forward transform) and reconstruction (inverse transform) [24, 26].

Let $\mathbf{x}$ be a discrete signal with $N = 2^J$ points (a sampled version of the analog signal $x(t)$). The discrete wavelet transform (DWT) of $\mathbf{x}$ is computed in a recursive cascade structure consisting of decimators $\downarrow 2$ and complementing low-pass filter h and high-pass filter g, which are uniquely associated with a wavelet [27, 28]. Figure 4 depicts a diagram of the filter bank structure.

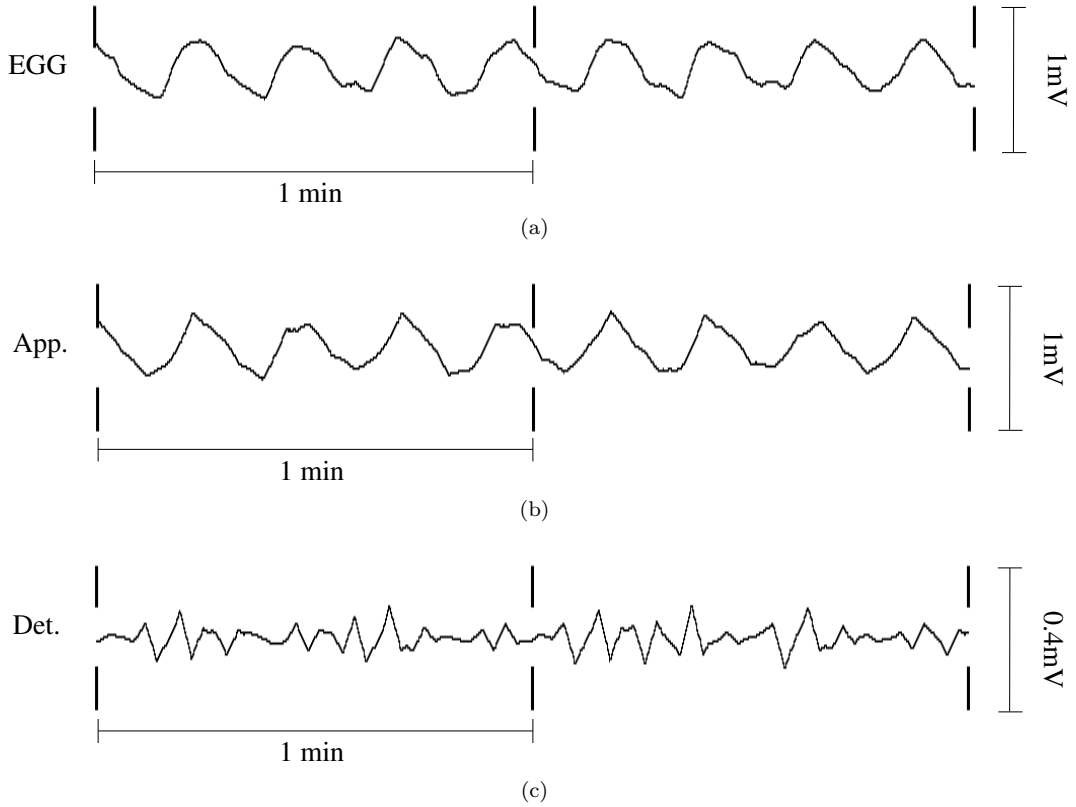

Figure 5: A 2-minute segment of a typical EGG signal in the basal state (a), decomposed into approximation (b) and detail (c) signals after the sixth iteration utilizing Mallat's pyramid algorithm. The wavelet utilized in this analysis was Daubechies-2.

At the end of the algorithm computation, a set of vectors is obtained

$$\left\{\mathbf{d}_1, \mathbf{d}_2, \ldots, \mathbf{d}_j, \ldots, \mathbf{d}_{J_0}, \mathbf{a}_{J_0}\right\}, \tag{3}$$

where J_0 is the number of decomposition scales of the DWT. This set of approximation and detail vectors represents the DWT of the original signal. Vectors $\mathbf{d}_j$ contain the DWT detail coefficients of the signal in each scale j. As j varies from 1 to J_0, a finer or coarser detail coefficient vector is obtained. On the other hand, the vector $\mathbf{a}_{J_0}$ contains the approximation coefficients of the signal at scale J_0. It should be noted that this recursive procedure can be iterated J times at most. Usually, the procedure is iterated $J_0 < J$ times. Depending on the choice of J_0, a different set of coefficients can be obtained. Observe that the discrete signal $\mathbf{x}$ and its DWT have the same length N. The inverse transformation can be performed using a similar recursive approach [28]. Generally, a signal can be subject to various wavelet decompositions. The analysis depends on (i) the choice of wavelet (filters h and g); and (ii) the number of decomposition levels (scales) J_0. Figure 5 shows an EGG signal in the basal state along with the associated approximation and detail signals, reconstructed from the respective approximation and detail vectors obtained as a result of wavelet-based decomposition utilizing Daubechies-2 wavelet [24].

A wavelet based compression scheme aims to satisfactorily represent an original discrete signal $\mathbf{x}$ with

as few DWT coefficients as possible [29–32]. One simple and effective way of doing that is to discard the coefficients that, under certain criteria, are considered insignificant. Consequently, the signal reconstruction is based on a reduced set of coefficients [29, 33].

In the present work the classic scheme for non-linear compression was used [29]. This procedure considers an *a posteriori* adaptive set, which keeps M wavelet transform coefficients that have the largest absolute values. A hard thresholding was utilized to set the remaining coefficients to zero. The number of coefficients M to be retained was determined according to the desired compression ratio CR, which was defined by

$$\mathrm{CR} = \frac{N}{M}, \tag{4}$$

where N and M are the number of wavelet transform coefficients of the original and the compressed signals, respectively.

Thus all three parameters in a wavelet compression scheme have been defined: (i) the number of scales; (ii) the compression ratio; and (iii) the type of the wavelet. However, before deriving approaches to determine each of these parameters, some additional issues need to be addressed.

2.2.2 Measurement of Distortion

The suggested assumption is that the normal and uncoupled EGG recordings have different typical energy distributions throughout the wavelet coefficients. Thus, depending on the signal (coupled or uncoupled), its energy is distributed differently among the wavelet transform coefficients. If the energy of the signal is spread evenly throughout the coefficients, fixing the number of discarded coefficients would result in greater distortions. By contrast, if the energy of the signal is concentrated in few wavelet coefficients, the odds are that they would survive the compression process, and consequently, the reconstructed signal would be closer to the original. Hence, for a fixed compression ratio, reconstructed signals present different distortions, depending on their energy distribution in the wavelet domain.

Therefore, to further the present analysis, it is necessary to introduce a quality assessment tool to compare the original discrete signal $\mathbf{x}$ with its reconstruction $\tilde{\mathbf{x}}$. Several measures that allow the evaluation of the effect of compression schemes have been suggested [34]. However, one of the most commonly used is the Percent Root-mean-square Difference (PRD) [30, 31, 34], which was utilized in the present study as a measure of distortion in the compression scheme. The PRD of two signals, $\mathbf{x}$ and $\tilde{\mathbf{x}}$, both of length N, is defined by:

$$\mathrm{PRD}(\mathbf{x}, \tilde{\mathbf{x}}) = \sqrt{\frac{\sum_{i=0}^{N-1}(x_i - \tilde{x}_i)^2}{\sum_{i=0}^{N-1} x_i^2}} \times 100\%. \tag{5}$$

2.3 Statistical Analysis

After computing the quality assessment parameter (PRD) for each canine EGG signal, the signals were grouped according to the state of the dog (basal, mild uncoupling, and severe uncoupling) and the recording channel. Significant statistical difference ($p < 0.05$) between the PRD values of compressed EGG signals obtained from the basal state and mild or severe gastric electrical uncoupling for a given channel was sought.

Since the EGG signals of the three groups were acquired from the same sixteen dogs, the assumption of data independence could be questioned. Consequently, a small-sample inference using straightforward

Table 1: Number of decomposition scales J_0 for some wavelets.

Wavelet	J_0
Daubechies-2	6
Daubechies-3	7
Coiflet-1	7

t-statistics might not be appropriate [35].

Paired statistical approaches, such as the Paired Difference test [35], were utilized to compare the PRD between two given groups of signals. Therefore, paired differences of the PRD's (ΔPRD) were computed. Since Paired Difference test can only be used when the relative frequency distribution of the population of differences is normal, the nonparametric Wilcoxon signed rank test could also be taken in consideration as an alternative [35].

To check the assumption of normal distribution of the ΔPRD samples, the Lilliefors (Kolmogorov-Smirnov) test of normality was utilized [36]. Whenever Lilliefors test verified that the difference between the samples satisfied a normal distribution, the Paired Difference test was utilized to compare the two groups. Otherwise, the less restrictive Wilcoxon signed rank test was employed.

2.4 Choice of Parameters

2.4.1 Number of Scales

In order to select the number of scales $J_0 \in \{1, \ldots, J\}$ of the wavelet transform decomposition, the following criterion was introduced: J_0 was chosen so that the coarsest approximation scale had a pseudo-frequency close to the canine EGG dominant frequency f_c of 4–6 cycles per minute [37].

The pseudo-frequency f_{pseudo} of a given scale j is

$$f_{\text{pseudo}} = \frac{f_\psi}{j \cdot T_s}, \qquad j = 1, \ldots, J, \tag{6}$$

where T_s is the sampling period (0.1 s) and f_ψ is the center frequency of a wavelet (the frequency that maximizes the magnitude of the Fourier transform of the wavelet) [28]. Consequently, the scale J_0 was selected which minimized the difference $(f_{\text{pseudo}} - f_c)$. Table 1 shows the number of decomposition levels for some common wavelets.

2.4.2 Compression Ratio

The selection of the compression ratio was performed by choosing the ratio that maximized the number of channels which exhibited statistically significant difference, when comparing the basal to the uncoupled groups of signals. In order to facilitate the selection process, a plot was constructed relating the compression ratio to the percentage of channels in which statistically significant difference was observed. This calculation was performed for two situations: (i) comparing basal state to mild electrical uncoupling; and (ii) comparing basal state to severe electrical uncoupling. Thus, the values of the compression ratio that delivered maximal percentage of detecting channels in both comparison cases were selected.

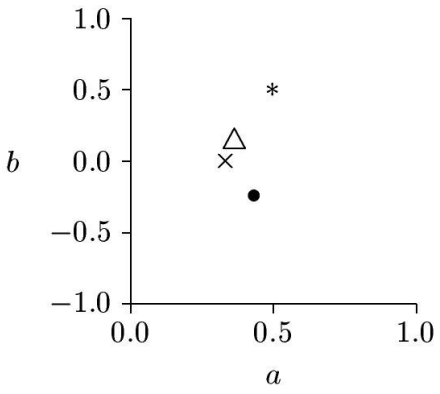

Figure 6: Parameterization plane (the axes are normalized by π). The coordinate points that correspond to Haar ($*$), Daubechies-2 ($\times$), Daubechies-3 ($\bullet$), and Coiflet-1 ($\triangle$) wavelets are shown.

In this study, three well-known wavelets were utilized, namely, Daubechies-2, -3, and Coiflet-1. The number of scales utilized was set accordingly (see Table 1).

2.4.3 Choice of Wavelet

Although there are numerous issues concerning the choice of wavelet for signal analysis [38], generally, a wavelet is better suited to a class of signals if the latter can be represented by as few wavelet coefficients as possible [24, 29]. Thus, wavelets which resemble the waveshape of the signal under analysis are often selected. In the context of the present study, a wavelet was sought that minimized the PRD between the original EGG signal and its reconstruction for a fixed compression ratio. If, for a given wavelet, the PRD associated with a compressed signal was minimal, then the surviving coefficients were considered to be better representing the original signal. Therefore, the selected wavelet was also more effectively "matched" to the signal under analysis when compared to other wavelets in consideration. However, the abundance of wavelets [27] makes such approach prohibitive. As a result, some constraints on the choice of wavelet were introduced.

It is well known that wavelets can be generated from discrete finite impulse response (FIR) filters [28]. In the present work, the analysis was limited to wavelets generated by FIR filters with length no greater than six coefficients. In this subset of wavelets one may find Haar, Daubechies-2, Daubechies-3, and Coiflet-1 wavelets, to name the most popular ones [24].

This restriction is quite convenient, since all FIR filters of length up to six that can be utilized to generate wavelets have simple parameterizations of their coefficients [39, 40]. For example, Pollen parameterization of 6-tap wavelet filters [39] has two independent variables $(a, b) \in [-\pi, \pi] \times [-\pi, \pi]$. Varying these two parameters, a filter that generates a new wavelet can be defined. Consequently, the Pollen parameterization defines a plane on which every point is connected to a wavelet [27]. In Figure 6, the parameterization plane is partially depicted and some wavelet positions are denoted.

Using the discussed compression scheme, one can compute a PRD value of a signal for each wavelet generated from a point with coordinates (a, b) on the parameterization plane. Doing so, a surface can be defined by the points (a, b, PRD). Thus, the minima of this surface correspond to the point coordinates (a, b) that generate a wavelet with good "matching" properties, since the PRD values at these minima are small. On the other hand, the maxima of this surface indicate higher values of PRD, consequently the reconstructed

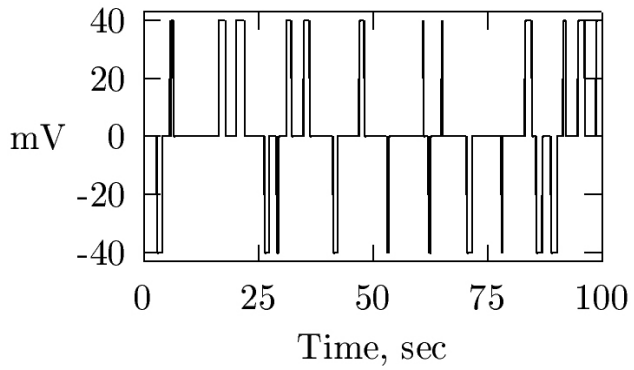

Figure 7: Square-wave test signal of random polarity.

signal from the compression is a poorer representation of the original.

2.4.4 Testing the Methodology

To verify the validity of the proposed methodology, it was applied to a square wave signal shown in Figure 7. It has been previously shown that the Haar wavelet matches this kind of signal and can offer a good representation [26]. Setting the compression ratio to 3 and the number of scales to 6, a PRD surface on the parameterization plane was constructed, resulting in the plot shown in Figure 8. A minimum of this surface occurs at the point $(\pi/2, \pi/2)$, which corresponds exactly to the Haar wavelet. Other minima are located on $(\pi/2, -\pi/2)$, $(\pi/2, 0)$, $(-\pi/2, \pi/2)$, $(-\pi/2, 0)$, and on the diagonal. All these regions also generate Haar-like wavelets. Therefore, the proposed procedure of finding the minima of the PRD surface could be applied to every EGG recording in the basal state, and a wavelet that would "match" normal EGG recordings could be defined. As a result, a set of point coordinates (a_i, b_i) could be determined on the parameterization plane, which minimizes the PRD for each normal canine EGG recording i. Figure 9 shows typical surfaces generated for basal canine EGG signals [41].

Taking the mean value of the minima, the best wavelet parameterization (a^*, b^*) could be defined. Thus, (a^*, b^*) generates a wavelet that on average "matches" best the normal EGG recordings.

3 Results

3.1 Determination of Parameters

3.1.1 Compression Ratio

The PRD values for all EGG recordings were computed using some selected wavelets (Daubechies-2, Daubechies-3, and Coiflet-1) and several compression ratios. Haar wavelet was not taken into consideration because it is not continuous, and offers poor approximations for smooth functions like the EGG signals [24]. Figure 10 shows the results of this procedure.

It is interesting to observe that percentage of channels in which statistically significant difference was found is highly dependent on the choice of compression ratio when comparing basal state and mild gastric electrical uncoupling groups. As the compression ratio increased, the resulting PRD sets from the two groups became

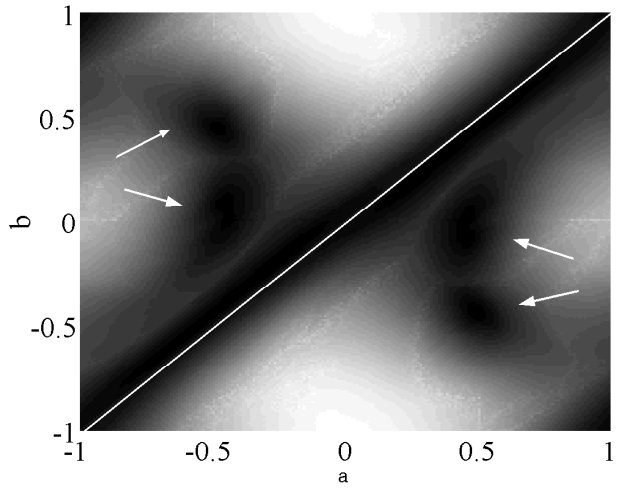

Figure 8: PRD surface on the parameterization plane resulting from processing the square-wave test signal with compression ration of 3. A gray scale is used to represent the PRD values. The darker areas are the minima of the PRD surface and coincide with the regions that generate Haar wavelets: the marked diagonal, $(0.5, -0.5)$, $(0.5, 0)$, $(-0.5, 0.5)$, and $(-0.5, 0)$ (indicated by the arrows). The axes are normalized by π.

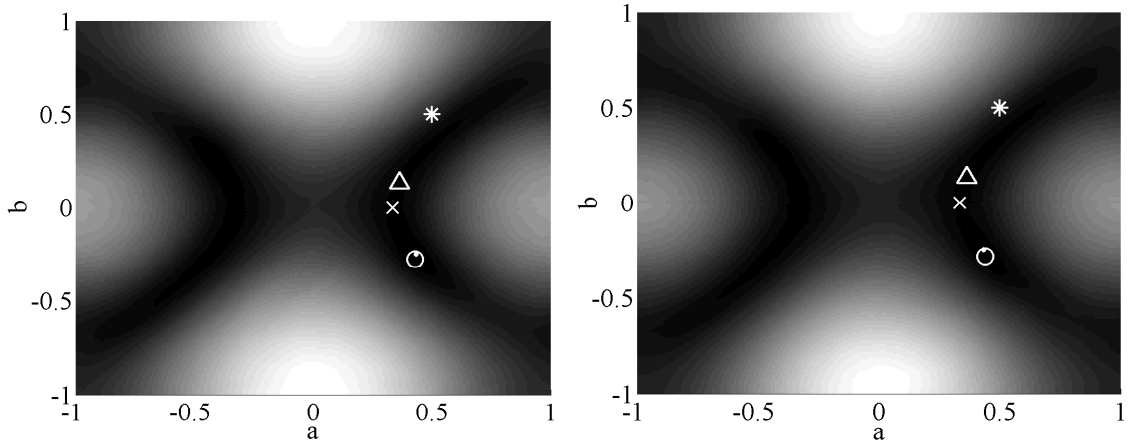

Figure 9: Plot generated after computing the PRD surface for all possible wavelets on the parameterization plane for two canine EGG signals in the basal state. The minimum value is depicted by a circle ($\circ$). The coordinate points that correspond to Haar ($*$), Daubechies-2 ($\times$), Daubechies-3 ($\bullet$), and Coiflet-1 ($\triangle$) wavelets are shown. The axes are normalized by π.

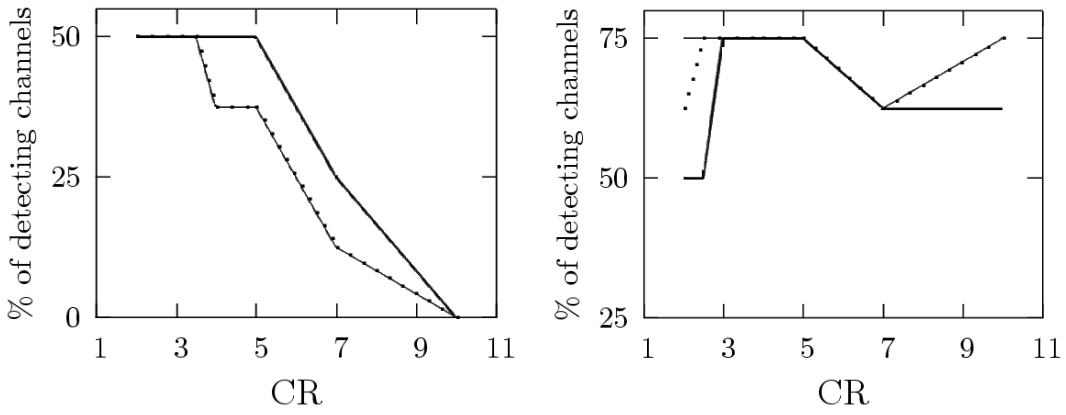

(a) Basal vs. Mild Electrical Uncoupling

(b) Basal vs. Severe Electrical Uncoupling

Figure 10: Compression ratio vs percentage of channels in which successful detection occurred ($p < 0.05$). Each curve displays the analysis for a specific wavelet: Daubechies-2 (thin solid line), Daubechies-3 (solid line), and Coiflet-1 (dotted line).

statistically less distinct, deteriorating the ability to discriminate between them. Figure 10(a) illustrates this behaviour.

On the other hand, the proposed algorithm is more prone to detect severe electrical uncoupling. Significant statistical difference ($p < 0.044$) between basal state and severe electrical uncoupling was observed in up to 6 out of 8 channels. Moreover, the percentage of channels where significance was consistently observed was relatively constant with respect to the change of compression ratio (Figure 10(b)).

Evidently, depending on the choice of wavelet, compression ratio range between 3 and 5 offered the best outcomes for both cases. Therefore, compression ratio of 3 was selected, which was the smallest compression ratio with which both plots achieved maximum values.

3.1.2 Wavelet

Setting the compression ratio to three, the specific values of $a^* = 0.43$ and $b^* = -0.26$ were determined, which were associated with the wavelet depicted in Figure 11 (bold curve). It is worth mentioning that the proposed wavelet was very similar to the classic Daubechies-3 wavelet. Since Daubechies-3 is (i) very similar to the proposed wavelet; and (ii) easily available in many software packages (e.g., Matlab (The Mathworks, Inc., Natick, MA, USA)), it was chosen instead of the proposed wavelet. Previous empirical findings [18] confirm this observation.

3.2 Statistics

Tables 2, 3 and 4 summarize the results when Daubechies-3 wavelet and compression ratio of 3 were utilized.

4 Discussion

In the employed model of gastric electrical uncoupling, as the myotomies were performed the electrical power produced by the intrinsic gastric generator was divided into two or three generators of lower electric

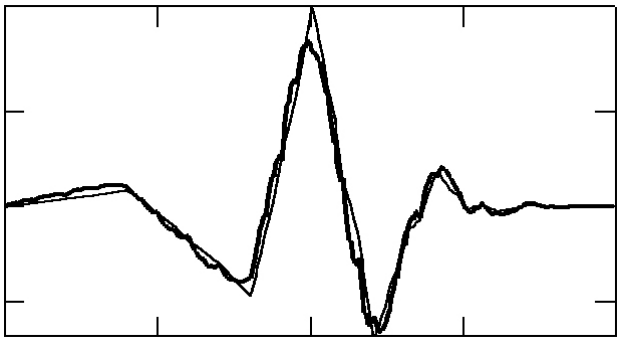

Figure 11: Comparison between the optimal wavelet (solid bold curve) obtained using the derived parameters a^* and b^*, and the standard Daubechies-3 wavelet (solid thin curve). The similarity between the two ones is clearly evident.

Table 2: Comparison between the PRD values in the basal state and mild gastric electrical uncoupling.

Channel	Statistics	ΔPRD Mean	ΔPRD SD	Significant?	p-value
7	Student	0.982161	1.844312	No	0.058226
8	Student	0.566675	0.679417	Yes	0.010919
9	Student	0.728762	1.137274	Yes	0.026378
10	Student	0.192864	1.314660	No	0.592370
11	Wilcoxon	1.347208	1.741442	Yes	0.000854
12	Student	1.186993	1.948825	Yes	0.033388
13	Wilcoxon	0.648649	1.532822	No	0.187622
14	Student	0.424109	1.643240	No	0.334474

Table 3: Comparison between the PRD values in the basal state and severe gastric electrical uncoupling.

Channel	Statistics	ΔPRD Mean	ΔPRD SD	Significant?	p-value
7	Student	0.924724	1.416927	Yes	0.029661
8	Student	0.755751	0.763789	Yes	0.005647
9	Student	0.596236	1.029897	Yes	0.049474
10	Student	0.306322	1.505244	No	0.428371
11	Student	0.813283	1.044165	Yes	0.015799
12	Student	0.972415	0.899240	Yes	0.001386
13	Student	0.634854	1.066521	Yes	0.044225
14	Student	0.467240	0.983946	No	0.112567

Table 4: Comparison between the PRD values in mild and severe gastric electrical uncoupling state.

Channel	Statistics	ΔPRD Mean	ΔPRD SD	Significant?	p-value
7	Student	0.011820	1.365449	No	0.973727
8	Student	0.074321	0.803788	No	0.744598
9	Student	−0.191332	1.317089	No	0.582588
10	Student	−0.169222	1.481669	No	0.676127
11	Student	−0.441275	1.605023	No	0.322378
12	Student	−0.304088	1.756426	No	0.513433
13	Student	0.044421	1.093672	No	0.877249
14	Student	−0.208983	1.242392	No	0.540001

power, according to the number of the circumferential cuts. Consequently, the signal-to-noise ratio of the recorded signal decreased and the influence of various external sources of disturbance became more expressive. Therefore, the energy of the EGG signal became more distributed throughout the wavelet coefficients, when compared to the signal in the basal state (single gastric generator). Due to the design of the proposed method, as the energy was distributed in more coefficients, the reconstruction error increased.

The evaluation of the reconstruction error of compressed canine EGG signals using the proposed wavelet technique was able to discriminate between induced severe gastric electrical uncoupling and the basal state in 75% of the EGG channels. The detection capability of the procedure was reduced when comparing the control group to the mild gastric uncoupling group but nevertheless, significant differences were observed in 4 out of 8 EGG channels (see Tables 2 and 3). This increase in sensitivity when detecting severe uncoupling is expected and reinforce previous findings [12, 14, 42]. Channels 8, 11 and 12 were recognized as the ones that presented the best overall performance in detecting uncoupling signals (p-values ranging from 0.0009 to 0.01). The site of such channels oversees the mid to distal corpus of the epigastric region. These electrode locations probably encompass fully electrical activity from all uncoupling regions. This observation emphasizes the appropriateness of using a multichannel EGG recording system.

A careful examination of Table 3 reveals that channels 9 and 13 have only borderline significance. A more conservative interpretation of the data (e.g., $p < 0.01$) would reduce the ability of the method to detect mild uncoupling to a single channel (#11), which, however, still represents a significant improvement in recognizing mild uncoupling, compared to previous findings [42].

Mild and severe gastric electrical uncoupling groups were statistically indistinguishable ($p > 0.05$). This indicates that, according to the proposed technique, EGG signals contain insufficient information to assess the level of gastric electrical uncoupling. In addition, when comparing mild and severe uncoupling, a non-consistent tendency of change in the reconstruction error was observed. This can be noted from the fluctuation of the sign of the mean reconstruction error in Table 4.

Previous works [12–14, 42] suggested that determinism, randomness, and chaos are dynamically blended in the EGG signals. The present investigation indicates that a single signal processing approach might be insufficient to provide an accurate assessment method for EGG recordings. Because of the complex dynamic nature of the EGG signal, various methods such as classical time-frequency analysis, wavelet theory, non-linear techniques, and biomagnetic field pattern recognition could be combined to provide sufficent data for an informed diagnostic decision. Indeed, such combined approach could be a key to converting electrogastrography into a reliable clinical tool.

5 Conclusion

A new wavelet analysis approach based on signal compression is proposed for the detection of mild and severe gastric electrical uncoupling in a canine model. Combining the results of the suggested wavelet compression scheme with a multichannel recording system and a comprehensive electrode configuration mapping the abdominal wall along the projection of the gastric axis, it was demonstrated that significant difference between the basal state and gastric electrical uncoupling can be detected in particular EGG channels. These channels are usually located along the abdominal projection of the mid to distal corpus axis.

Acknowledgments

This work was supported by the Natural Sciences and Engineering Research Council of Canada (NSERC) and the National Council for Scientific and Technological Development (CNPq, Brazil).

References

[1] J. H. Szurszewski, *Physiology of the Gastrointestinal Tract*. New York: Raven Press, 1981, ch. Electrical Basis for Gastrointestinal Motility, pp. 1435–1466.

[2] E. E. Daniel, B. L. Bardakjian, J. D. Huizinga, and N. E. Diamant, "Relaxation oscillator and core conductor models are needed for understanding of GI electrical activities," *American Journal of Physiology: Gastrointestinal and Liver Physiology*, vol. 226, no. 3, pp. 475–482, 1994.

[3] M. Bortolotti, "Electrogastrography: A seductive promise, only partially kept," *The American Journal of Gastroenterology*, vol. 93, no. 10, pp. 1791–1794, Oct. 1998.

[4] J. D. Z. Chen, J. Pan, and R. W. McCallum, "Clinical significance of gastric myoelectrical dysrhythmias," *Digestive Diseases and Sciences*, vol. 13, no. 5, pp. 275–290, Sep. 1995.

[5] J. D. Z. Chen, W. R. Stewart Jr., and R. W. McCallum, "Spectral analysis of episodic rhythmic variations in cutaneous electrogastrogram," *IEEE Transactions on Biomedical Engineering*, vol. 40, no. 2, pp. 128–135, Feb. 1993.

[6] H. P. Parkman, W. L. Hasler, J. L. Barnett, and E. Y. Eaker, "Electrogastrography: a document prepared by the gastric section of the american motility society clinical GI motility testing task force," *Neurogastroenterology and Motility*, vol. 15, pp. 89–102, 2003.

[7] C. H. You and W. Y. Chey, "Study of electromechanical activity of the stomach in humans and dogs with particular attention to tachygastria," *Gastroenterology*, vol. 86, pp. 1460–1468, 1986.

[8] M. P. Mintchev and K. L. Bowes, "Do increased electrogastrographic frequencies always correspond to internal tachygastria?" *Annals of Biomedical Engineering*, vol. 25, pp. 1052–1058, 1997.

[9] L. A. Bradshaw, A. G. Myers, A. Redmond, J. P. Wikswo, and W. O. Richards, "Biomagnetic detection of gastric electrical activity in normal and vagotomized rabbits," *Neurogastroenterology and Motility*, vol. 15, no. 5, pp. 475–482, Oct. 2003.

[10] N. G. Publicover and K. M. Sanders, "Are relaxation oscillators an appropriate model of gastrointestinal electrical activity?" *American Journal of Physiology: Gastrointestinal and Liver Physiology*, vol. 256, no. 2, pp. 265–274, 1989.

[11] A. J. P. M. Smout, E. J. Van Der Schee, and J. L. Grashuis, "What is measured in electrogastrography?" *Digestive Diseases and Sciences*, vol. 25, no. 3, pp. 179–186, Mar. 1980.

[12] M. P. Mintchev, S. J. Otto, and K. L. Bowes, "Electrogastrography can recognize gastric electrical uncoupling in dogs," *Gastroenterology*, vol. 112, pp. 2006–2011, 1997.

[13] M. P. Mintchev, A. Stickel, and K. L. Bowes, "Dynamics of the level of randomness in gastric electrical activity," *Digestive Diseases and Sciences*, vol. 43, no. 5, pp. 953–956, May 1998.

[14] J.-Y. Carré, A. Høst-Madsen, K. L. Bowes, and M. P. Mintchev, "Dynamics of the level of deterministic chaos associated with gastric electrical uncoupling in dogs," *Medical & Biological Engineering & Computing*, vol. 39, pp. 322–329, 2001.

[15] L. A. Bradshaw, J. K. Ladipo, J. P. Wikswo, Jr., and W. O. Richards, "The human vector magnetogastrogram and magnetoenterogram," *IEEE Transactions on Biomedical Engineering*, vol. 46, no. 8, pp. 959–970, Aug. 1999.

[16] L. A. Bradshaw, A. Myers, J. P. Wikswo, and W. O. Richards, "A spatio-temporal dipole simulation of gastrointestinal magnetic fields," *IEEE Transactions on Biomedical Engineering*, vol. 50, no. 7, pp. 836–847, Jul. 2003.

[17] X. Xie and H. H. Sun, "Sinusoidal time-frequency wavelet family and its application in electrogastrographic signal analysis," in *Proceedings of the 20th Annual International Conference of the IEEE Engineering in Medicine and Biology Society*, vol. 3, Hong Kong, China, 1998, pp. 1450–1453.

[18] C. Ryu, K. Nam, S. Kim, and D. Kim, "Comparison of digital filters with wavelet multiresolution filter for electrogastrogram," in *Proceedings of the Second Joint BMES/EMBS Conference*, Houston, TX, Oct. 2000, pp. 137–138.

[19] J. Liang, J. C. Cheung, and J. D. Z. Chen, "Noise detection and denoising on electrogastrography using nonorthogonal multiresolution wavelet analysis," in *Proceedings of the 18th Annual International Conference of the IEEE Engineering in Medicine and Biology Society*, vol. 3, Amsterdam, Netherlands, 1996, pp. 1039–1040.

[20] H. Liang and Z. Lin, "Stimulus artifact cancellation in the serosal recordings of gastric myoelectric activity using wavelet transform," *IEEE Transactions on Biomedical Engineering*, vol. 49, no. 7, pp. 681–688, Jul. 2002.

[21] W. Qiao, H. H. Sun, W. Y. Chey, and K. Y. Lee, "Continuous wavelet analysis as an aid in the representation and interpretation of electrogastrographic signals," in *Proceedings of the Fifteenth Southern Biomedical Engineering Conference*, Dayton, USA, Mar. 1996, pp. 140–141.

[22] N. Mirizzi and U. Scafoglieri, "Optimal direction of the electrogastrographic signal in man," *Medical & Biological Engineering & Computing*, vol. 21, no. 4, pp. 385–389, Jul. 1983.

[23] M. A. M. T. Verhagen, L. J. Van Schelven, M. Samsom, and A. J. P. M. Smout, "Pitfalls in the analysis of electrogastrographic recordings," *Gastroenterology*, vol. 117, no. 2, pp. 453–460, 1999.

[24] S. G. Mallat, *A Wavelet Tour of Signal Processing*, 2nd ed. Academic Press, 1999.

[25] M. Unser and T. Blu, "Wavelet theory demystified," *IEEE Transactions on Signal Processing*, vol. 51, no. 2, pp. 470–483, Feb. 2003.

[26] H. M. de Oliveira, *Análise de Sinais para Engenheiros: Uma Abordagem Via Wavelets*. São Paulo: Manole Pub., 2004.

[27] O. Bratteli and P. E. T. Jorgensen, *Wavelets Through A Looking Glass: The World of the Spectrum*. Boston: Birkhäuser, 2002.

[28] M. Misiti, Y. Misiti, G. Oppenheim, and J.-M. Poggi, *Wavelet Toolbox User's Guide*, 2nd ed. New York: The MathWorks, Inc., 2000.

[29] M. Vetterli, "Wavelets, approximation, and compression," *IEEE Signal Processing Magazine*, vol. 5, pp. 59–73, Sep. 2001.

[30] A. Chagas, E. Da Silva, and J. Nadal, "ECG data compression using wavelets," in *Computers in Cardiology*, Sep. 2000, pp. 423–426.

[31] Z. Lu, D. Y. Kim, and W. Pearlman, "ECG signal compression with a new wavelet method," in *Proceedings of the First Joint BMES/EMBS Conference*, Atlanta, GA, Oct. 1999, p. 955.

[32] M. J. Watson, A. Liakopoulos, D. Brzakovic, and C. Georgakis, "Wavelet techniques in the compression of process data," in *Proceedings of the American Control Conference*, Seattle, USA, Jun. 1995, pp. 1265–1269.

[33] M. Unser and A. Aldroubi, "A review of wavelets in biomedical applications," *Proceedings of the IEEE*, vol. 84, no. 4, pp. 626–638, Apr. 1996.

[34] R. Besar, C. Eswaran, S. Sahib, and R. J. Simpson, "On the choice of the wavelets for ECG data compression," in *Proceedings of the International Conference on Acoustics, Speech, and Signal Processing*, Istanbul, Turkey, Jun. 2000, pp. 1011–1014.

[35] G. W. Snedecor and W. G. Cochran, *Statistical Methods*, 6th ed. Iowa State University Press, 1967.

[36] T. Gonzalez, S. Sahni, and W. R. Franta, "An efficient algorithm for the Kolmogorov-Smirnov and Lilliefors tests," *ACM Transactions on Mathematical Software*, vol. 3, no. 1, pp. 60–64, Mar. 1977.

[37] M. P. Mintchev, A. Girard, and K. L. Bowes, "Nonlinear adaptive noise compensation in electrogastrograms recorded from healthy dogs," *IEEE Transactions on Biomedical Engineering*, vol. 47, no. 2, pp. 239–248, Jan. 2000.

[38] J. O. Chapa and R. M. Rao, "Algorithms for designing wavelets to match a specified signal," *IEEE Transactions on Signal Processing*, vol. 48, no. 12, pp. 3395–3406, Dec. 2000.

[39] A. H. Tewfik, D. Sinha, and P. Jorgensen, "On the optimal choice of a wavelet for signal representation," *IEEE Transactions on Information Theory*, vol. 38, no. 2, pp. 747–765, Mar. 1992.

[40] H. Zhou and A. H. Tewfik, "Parametrization of compactly supported orthonormal wavelets," *IEEE Transactions on Signal Processing*, vol. 41, no. 3, pp. 1428–1431, Mar. 1993.

[41] R. A. Gopinath, J. E. Odegard, and C. S. Burrus, "Optimal wavelet representation of signals and the wavelet sampling theorem," *IEEE Transactions on Circuits and Systems—II: Analog and Digital Signal Processing*, vol. 41, no. 4, pp. 262–277, Apr. 1994.

[42] C. P. Sanmiguel, M. P. Mintchev, and K. L. Bowes, "Dynamics of level of randomness of electrogastrograms can be indicative of gastric electrical uncoupling in dogs," *Digestive Diseases and Sciences*, vol. 44, no. 3, pp. 523–528, Mar. 1999.